PHYSICS AND CHEMISTRY OF SOLID STATE
V. 26, No. 2 (2025) pp. 447-456
Section: Physics

DOI: 10.15330/pcss.26.2.447-456

Vasyl Stefanyk Precarpathian National University

ФІЗИКА І ХІМІЯ ТВЕРДОГО ТІЛА
Т. 26, № 2 (2025) С. 447-456
Фізико-математичні науки

PACS: 75.75. + a, 81.07. – b, 61.72.uf, 76.30.-v, 78.30.Am, 78.55.-m

ISSN 1729-4428 (Print)
ISSN 2309-8589 (Online)

O.V. Kovalenko[1], V.Yu. Vorovsky[1], N.I. Berezovska[2,3], I.M. Dmytruk[2,3], D.V. Korbutyak[4], V.O. Yukhymchuk[4]

Optical, structural and radiospectroscopic studies of ZnO/MnO nanostructures synthesized by ultrasonic spray pyrolysis

[1]*O. H. Dnipro National University, Dnipro, Ukraine, kovalenko.dnu@gmail.com;*
[2]*Taras Shevchenko National University of Kyiv, Kyiv, Ukraine;*
[3]*Institute of Physics, NAS of Ukraine, Kyiv, Ukraine;*
[4]*V. Lashkaryov Institute of Semiconductor Physics, NAS of Ukraine, Kyiv, Ukraine*

The technology for the synthesis of nanocrystals (NCs) of pure ZnO and ZnO doped with a magnetic Mn impurity in concentrations of 2% and 4% by ultrasonic spray pyrolysis has been developed. The structural, morphological and optical properties of syntesied ZnO NCs have been studied with methods of X-ray diffraction, scanning electron microscopy, electron paramagnetic resonance (EPR), spectroscopy of Raman scattering and photoluminescence. The defective near-surface layer in ZnO:Mn NCs has been identified based on the analysis of the EPR spectra. Thermal annealing of samples at T = 850°C leads to the ordering of the crystal structure of ZnO:Mn NCs. The solubility limit of the Mn impurity is less than 2%. Raman spectra analysis has revealed that ZnO:Mn NCs are covered with $ZnMn_2O_4$ and d--MnO_2 shells. A significant increase in the intensity of exciton photoluminescence for ZnO NCs caused by the improvement of the structural perfection of NCs is to be a result of increasing the liquid flow rate to 40 l/h during the synthesis process. Thus, the optimal technological regimes to form high-quality, structurally perfect ZnO NCs can be elaborated by changing the liquid flow rate during the synthesis process.

Keywords: Zinc oxide, Nanocrystals, Magnetic Impurities, Defects, Ultrasonic spray pyrolysis, X-ray diffraction, Electron paramagnetic resonance, Raman scattering, Photoluminescence.

Received 25 May 2025; Accepted 30 June 2025.

Introduction

Semiconductor nanocrystals (NCs) are attracting a lot of attention due to their exceptional properties which appear when they are doped. One of the most important changes that occur when NCs are doped with magnetic impurities is the appearance of magnetic properties in the original non-magnetic material. For example, in the case of $A^{II}B^{VI}$ NCs, the addition of magnetic impurities such as manganese (Mn), cobalt (Co) or iron (Fe) can lead to the formation of ferromagnetic properties in the material. The ability to control the magnetic properties of $A^{II}B^{VI}$ NCs via an external magnetic field opens up the possibility of using them in magnetic detectors and sensors. This can be useful for measuring magnetic fields with high sensitivity and accuracy. In addition, the optical properties of nanocrystals change that is reflected in their spectral characteristics. Changes in light absorption, fluorescence and scattering depending on the magnetic field open up the possibilities for the creation of magneto-optical devices. Magnetic impurities can affect the electronic structure of $A^{II}B^{VI}$ NCs, changing their electronic properties. For example, they can affect the energy levels in the band gap of a material, affecting its conductivity and electrical resistance. Some research is also being conducted in the field of using $A^{II}B^{VI}$ NCs in quantum computing, where their unique quantum2 properties c_an be used to create quantum bits (qubits) and perform quantum operations.

In present work, the study of ZnO NCs doped with a magnetic Mn impurity was carried out. Zinc oxide is a multifunctional semiconductor with a wide band gap

(3.37 eV at 300 K) and large exciton binding energy of ~60 meV.

Due to its versatile properties, such as transparency in the visible region, high electrochemical stability, non-toxicity, radiation stability, and UV generation at room temperature, ZnO nanostructures are promising candidates for the functional components of devices and materials on photonic crystals, gas sensors, LEDs, solar cells, lasers, varistors, and photoelectrochemical cells, as well as for use in biosensors, bioimaging, drug delivery and other similar biological applications.

ZnO nanocrystals are synthesised by various methods, including p*recipitation* method from *zinc nitrate and ammonium carbonate* [1], sol-gel technique [2], microwave plasma sputtering on quartz substrates with controlled size distribution [3], modified polyol method [4], synthesis with Zn(OH)2 by hydrothermal method [5], electromagnetic levitation gas condensation method [6], ultrasonic spray pyrolysis method [7,8], cryochemical synthesis method [9], etc.

In recent years, interest in the green synthesis of ZnO:Mn NCs for antibacterial and photocatalytic applications has increased [10]. ZnO nanoparticles doped with manganese are obtained using reducing and blocking components of *W. coagulans* plant extract. In [10], ZnO:Mn NPs were fabricated, their characteristics were studied, and a biological evaluation was performed. It was found that the fabricated NCs are more stable, keep their crystallinity, and showed high antibacterial and photocatalytic activity against some bacteria and methylene blue dye, respectively. ZnO:Mn nanocrystals obtained from a biological source are characterised by minimal use of dangerous chemicals. The controlled synthesis of environmentally friendly, biocompatible ZnO:Mn NCs indicates the prospect of their use in various biomedical fields.

I. Synthesis of ZnO and ZnO:Mn nanocrystals by ultrasonic spray pyrolysis

The method of ultrasonic spray pyrolysis is based on the thermal decomposition of the aerosol droplets of the starting solution during their passage through the thermal zone of the furnace. The thermal decomposition takes place in the atmosphere of the carrier gas, and the final product is separated on a mesh filter heated to appropriate temperature. An aqueous solution of zinc nitrate - Zn(NO3)2-6H2O with a concentration of 0.15 M was used for the synthesis of ZnO and ZnO:Mn nanocrystals by this method. The doping of the samples with an Mn impurity was carried out by adding a solution of manganese nitrate - $Mn(NO_3)_2$-$6H_2O$ to the basic zinc nitrate solution, which corresponded to an atomic concentration of Mn in ZnO:Mn NCs of 2% and 4%, respectively.

During the synthesis, air was used as the carrier gas, the solution flow rate was 20 l/h, the synthesis temperature was T = 550^0C, and the duration of the solution droplets in the thermal zone was 6 ÷ 8 s. The ultrasonic solution sprayer was operated at 1.7MHz. The resulting powder was separated from water vapor and other synthesis products on a stainless steel mesh filter heated to T = 230-250 °C. During synthesis in the furnace zone, thermal decomposition of solution droplets occurs with the formation of ZnO:Mn NCs in accordance with the following chemical equations:

$$2(Zn(NO_3)_2) \xrightarrow{T=550°C} 2ZnO + 4NO_2 + O_2 \quad (1)$$

$$Mn(NO_3)_2 \xrightarrow{T=550°C} MnO_2 + 2NO_2 \quad (2)$$

The synthesis of ZnO:Mn NCs by this method occurs in the volume of a microdroplet with a size of D = 1.0 ÷ 2.0 μm during its passage through the thermal zone of the furnace. This allows you to reduce the influence of external factors during synthesis and obtain a pure product. In this case, the following processes sequentially occur in the solution droplet: evaporation of the solvent (water) from the droplet surface to form a solid shell, drying of the substance, synthesis of NCs by thermal decomposition of components, as well as simultaneous thermal treatment of the synthesized NCs (Fig. 1).

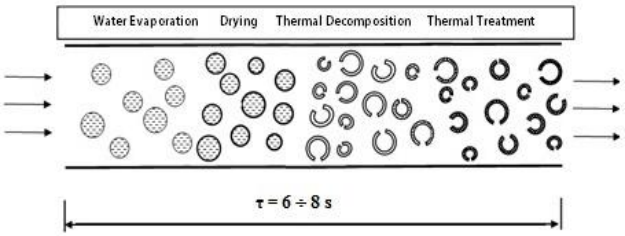

Fig. 1. Stages of ZnO:Mn nanoparticles synthesis by ultrasonic spray pyrolysis method.

Dry granules are the final product of the synthesis. They are mechanically unstable, easily crushed, and consist of ZnO:Mn NCs. The dimensions of the NCs calculated by X-ray diffraction analysis according to the Debye-Scherrer method were d = 36÷40 nm. The images of the particles of the synthesized powders obtained using a scanning electron microscope REMMA-102-02 is shown in Fig. 2. The presented photographs show that the synthesized particles have a spherical shape with a hole. They are hollow inside that is the result of leakage of gaseous products of thermal decomposition reactions. The size of spherical particles increases from 0.3÷1.0 μm to 1.0÷3.0 μm with increasing zinc nitrate concentration from 0.15M to 0.3M, respectively (Fig. 2).

The X-ray diffraction patterns of the synthesized samples of ZnO and ZnO:Mn NCs with Mn concentrations of 2% and 4% are shown in Fig. 3a. They do not exhibit reflections from impurity phases. This result indicates that single-phase compounds are obtained, but this conclusion cannot be final, taking into account the limited sensitivity of the X-ray diffraction method. The crystal structure of ZnO and ZnO:Mn NCs is hexagonal wurtzite (according to the standard JCPDS card: 36-1451). An increase of the Mn concentration leads to a decrease in the crystalline quality of the samples - the intensity of the reflections decreases. The lines become broader. This result may be caused by the fact that during non-equilibrium short-term synthesis, not all Mn impurity ions have time to be incorporated into the ZnO crystal lattice.

A certain number of impurity ions are pushed onto the surface of the NC, where a defect shell is formed around the crystalline core of the NC.

Analysis of the obtained X-ray diffraction patterns shows that the positions of the reflections are shifted relative to the standard values for ZnO towards large diffraction angles. The example of the analysis of (101) reflections (Fig. 3b) shows that the shift of the reflections of the X-ray diffraction pattern of the ZnO sample relative to the standard ($2\Theta_{101}$ = 42.36°) has the value $\Delta(2\Theta)$ = 0.34°. Taking into account the Wolf-Bragg formula such shift of reflections indicates a change in interplanar distances, which, in turn, causes the appearance of deformation stresses in the crystal lattice of the NC. A shift in the positions of the reflections with increasing Mn concentration relative to the sample of synthesized ZnO NCs towards small diffraction angles is also observed. For the sample of ZnO:Mn - 4% NCs the shift reaches the value $\Delta(2\Theta)$ = 0.1°.

Calculation of structural parameters of ZnO, ZnO:Mn-2% and ZnO:Mn-4% samples is given in Table 1. It is necessary to pay attention to the fact that the volume of the unit cell V increases during doping with Mn impurity. This is explained by the fact that during doping, Zn^{2+} ions are replaced in the crystal lattice sites by Mn^{2+} ions, which have a larger ionic radius: the ionic radius of Mn^{2+} (0.83 Å) is larger than that of Zn^{2+} (0.74 Å).

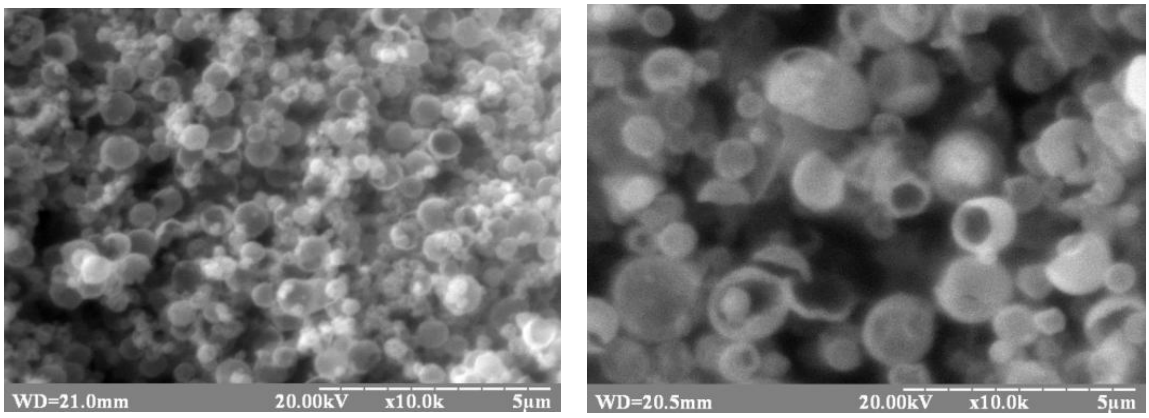

Fig. 2. Scanning electron microscopy images of ZnO powder particles obtained from 0.15 M zinc nitrate solutions with a concentration of 0.15 M (a) and 0.3 M (b).

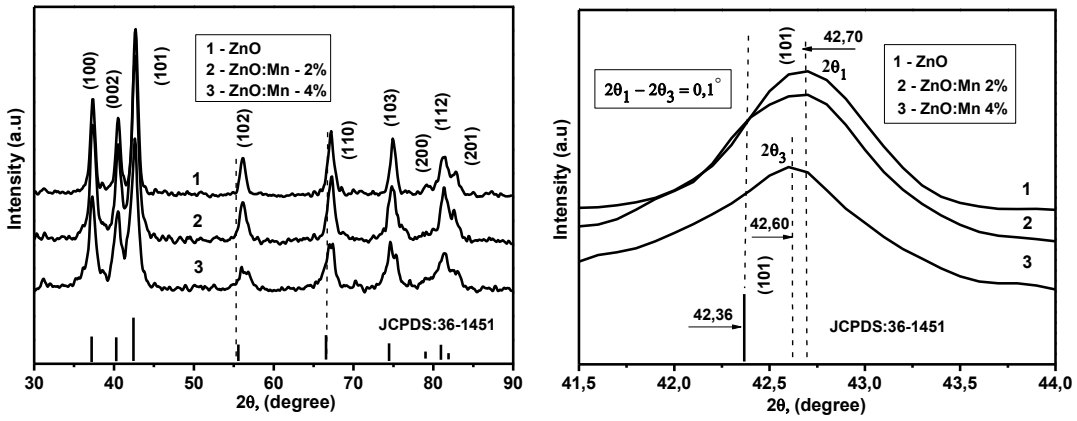

а б

Fig. 3. X-ray diffraction patterns of samples synthesized at a temperature of T = 550°C (a), shift of reflection (101) (b): 1 - ZnO sample, 2 - ZnO:Mn-2%, 3 - ZnO:Mn-4%.

Table 1.

Structural parameters of ZnO, ZnO:Mn - 2% and ZnO:Mn - 4% samples.

Sample	Designation of reflections, Hkl	Reflection angles, 2Θ°	Angular extension of reflections, β°	Crystal lattice parameters		Unit cell volume, *V*, Å^3	Strain tensor, ε×10^{-4}
				a, Å	*c*, Å		
ZnO	100	37,366	0,859	3,2307	-	46,753	5,9
	002	40,499	0,933	-	5,1725		
ZnO:Mn 2 %	100	37,346	0,730	3,2317	-	46,780	17,5
	002	40,505	0,714	-	5,1718		
ZnO:Mn 4 %	100	37,270	0,914	3,2386		46,985	51,9
	002	40,495	1,050		5,1728		

II. Study of EPR spectra in ZnO:Mn NCs

The electron paramagnetic resonance (EPR) method has the relevant advantages among the methods of studying the crystal structure of semiconductors due to its high resolution and sensitivity. This, in turn, makes it possible to obtain information about the local environment of the impurity ion and to determine the influence of deformation stresses on this state, which leads to changes in the parameters of the EPR spectrum. The EPR method allows to detect the presence of ferromagnetic clusters in the samples. In [11] it was shown that the resonance line of the EPR spectrum in the region of low magnetic field values may be a consequence of the presence in the sample of a large number of acceptor-type defects, which form ferromagnetic clusters due to exchange interaction Mn^{2+} impurity ions.

In ZnO NCs, the Mn^{2+} impurity can be located at the sites of the crystal lattice, which leads to the appearance of six ultrafine structure (UFS) lines of Mn^{2+} ions in the EPR spectra. In addition, another part of the impurity can be located between the crystal lattice sites and form clusters. This case leads to the appearance of a broad absorption line in the EPR spectra, which is due to the dipole interaction between Mn^{2+} ions in the clusters. That is why the EPR method is often used to determine the position of ions in the crystal lattice and to study the process of doping ZnO with Mn impurity [12].

We have studied the EPR spectra of ZnO:Mn NCs with manganese impurity concentrations of 2, 4, and 8% (Fig. 4a). This set of samples allowed us to analyze changes in the EPR spectra with increasing impurity concentration. The EPR spectra of the samples were studied using RADIOPAN SE/X 2543 radio spectrometer. The synthesized samples were exposed to heat treatment (HT) in air at T = 850°C for 1 h. Such HT also significantly affected the EPR spectra (Fig. 4b).

Analysis of the obtained results indicates that the EPR spectra of ZnO:Mn NCs before annealing (Fig. 4a) consist of a broad background absorption line caused by the magnetic dipole-dipole interaction of manganese ions and six UFS lines of Mn^{2+} ions, which isovalently replace Zn^{2+} ions in the ZnO crystal lattice. An increase of the concentration of the Mn impurity leads to an increase of the background line intensity and a decrease of the amplitudes of UFS lines, which is explained by an increase of the number of interstitial Mn ions and an enhancement of their magnetic dipole-dipole interaction. This behaviour may indicate that during the synthesis of ZnO the doping occurs partially. Despite the increase of the impurity concentration not all Mn^{2+} ions replace Zn^{2+} ions in the ZnO crystal lattice. They are located in large quantities on the surface of the NCs, forming a defective shell. The analysis of the EPR spectra of the synthesized samples gives a reason to believe that there is a defective near-surface layer in the ZnO:Mn NCs. The presence of a broad background absorption line in the EPR spectrum of the ZnO:Mn-2 % NC sample also indicates that the solubility limit of the Mn impurity is less than 2 %. The heat treatment of the samples leads to an increase in the intensity of the UFS lines of Mn^{2+} ions and almost to the disappearance of the broad background absorption line (Fig. 4b). This fact may demonstrate that due to thermal diffusion, almost all Mn^{2+} ions are located in the ZnO crystal lattice. The crystal structure of the sample after annealing at T = 850˚C does not have a significant number of structural defects. The near-surface layer disappears, the crystal structure of the NCs becomes ordered, and only the UFS lines of Mn^{2+} ions are recorded in the EPR spectra. Careful analysis of the EPR spectrum ZNO: Mn-2% before and after HT (Fig. 5) confirms the presence of heterogeneity of the crystalline structure of the sample. This conclusion is based on the fact that in samples before annealing, the UFS lines of Mn^{2+} ions are double. They consist of the superposition of two SI and SII spectra. The shift between the spectra is $\Delta H = 3.9$ mT. The SI spectrum is caused by Mn^{2+} ions which isovalently replace Zn^{2+} ions in the sites of the ZnO NCs lattice. The SII spectrum is associated with Mn^{2+} ions, which can be located in a deformed surface layer [13]. The width of SI spectrum is $\Delta H_1 = 39.52$ mT, the ultrafine interaction constant A = 7.9 mT. The width of the SII spectrum is $\Delta H_2 = 41.65$ mT, the constant A = 8.3 mT. After annealing, the intensity of the UFS lines of the EPR spectrum is redistributed in favour of the SI spectrum. The SII spectrum practically disappears, which indicates the diffusion of Mn^{2+} ions from the surface layer into the volume of ZnO NCs and the disappearance of the

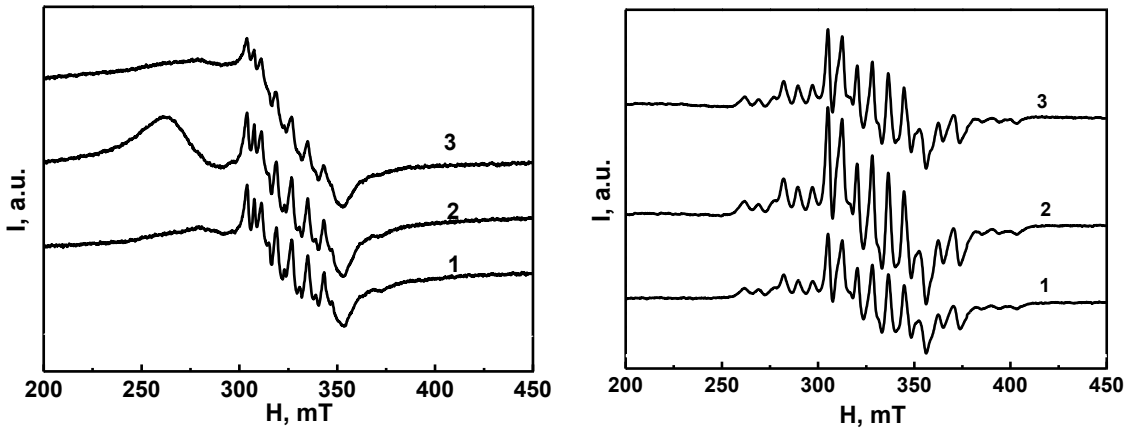

а) б)

Fig. 4. EPR spectra of ZnO:Mn NC samples before annealing (a) and after annealing at T= 850°C (b), Mn impurity concentration: 2% - (1), 4% - (2), 8% - (3).

defective shell.

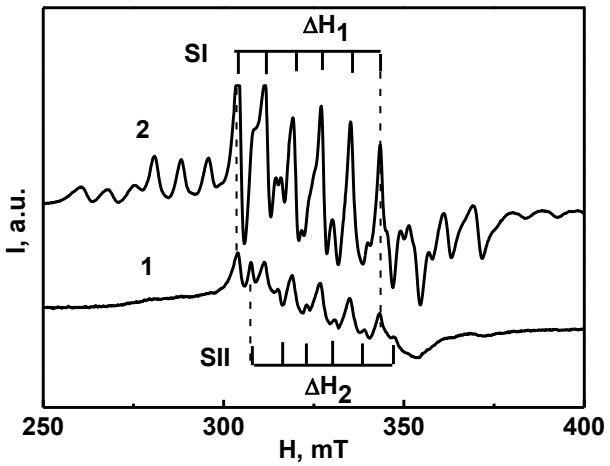

Fig. 5. EPR spectra of nO: Mn - 2 % NCs before annealing (1) and after annealing (2).

During the analysis of the procedure of rebuilding the defective shell of ZnO:Mn NCs with a manganese concentration of 2%, changes in the EPR spectrum during HT of the samples in air [14] at temperatures T = 550˚C and T = 850˚C (Fig. 6) were also investigated. Additionally, their HT was carried out in a flow of a mixture of hydrogen and nitrogen gases in the ratio $H_2/N_2 \sim 1/3$ at a temperature of T = 550˚C. HT was short-term to prevent increase of the size of the NCs. It lasted for 20 min. At the same time, the samples were cooled in the cold zone of the furnace for 15 min. in a flow of gaseous nitrogen.

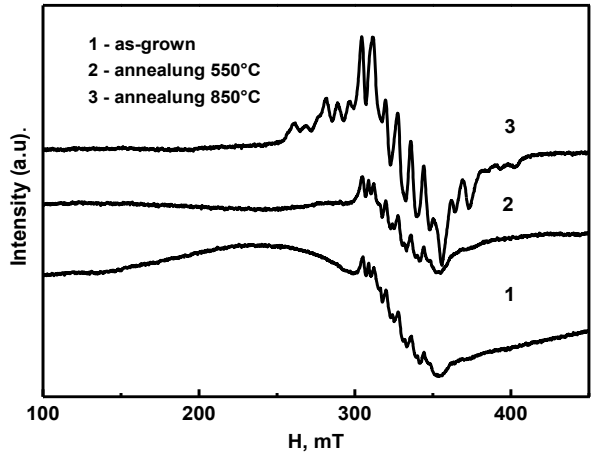

Fig. 6. EPR spectra of ZnO:Mn (2%) NCs: 1 – before annealing in air; 2 – after annealing at T = 550˚C; 3 – after annealing at T = 850˚C.

It is shown that in the EPR spectrum of the sample before annealing (Fig. 6), a broad, structureless line is recorded. It is located in the region of low magnetic field values H ~ 250 mT. Such absorption line may be a ferromagnetic resonance line due to the presence of a ferromagnetic phase in the sample. According to [13] this phase is a feature of the presence of ferromagnetic resonance in the samples at room temperature. After annealing of NCs at T = 550°C and T = 850°C, this line gradually disappears due to a decrease of the number of intrinsic defects. Analysis of the EPR spectra before and after annealing revealed that HT of the samples leads to a decrease of the intensity of the broad background line and an increase of the intensity of the UFS lines of Mn^{2+} ions (Fig. 6). This phenomenon occurs due to a decrease of the number of interstitial, Mn impurity ions that participate in the dipole exchange interaction. During HT some of them, as a result of thermal diffusion, begin to participate in the doping of ZnO NCs, occupying places in the crystal lattice sites that increases the intensity of the UFS lines.

Thus, it is shown that the process of doping with Mn impurity continues during HT, the defect content of the samples decreases. The location of the doping Mn^{2+} impurity ions in the volume of ZnO NCs becomes more homogeneous. In its turn, this effect causes a significant reduction in the thickness of the defective near-surface layer. Long-term annealing of the sample will lead to its complete disappearance.

It has been experimentally shown that this near-surface defect layer lost after HT can be restored by modifying the NC surface, for example, by annealing in a hydrogen environment [15].

The EPR spectrum of the sample after HT at T = 550 °C in an atmosphere with hydrogen is shown in Fig. 7. This sample was subjected to a short-term HT in air at T = 850˚C before the annealing. The amplitude of the background absorption line of the EPR spectrum increases in several times as a result of HT in hydrogen atmosphere. This is due to a significant change of the defective near-surface layer of the NC. At the same time, the line width of the central part of the EPR spectrum decreases from the value $\Delta H_1 = 39.52$ mT to $\Delta H_2 = 29.10$ mT. In ZnO semiconductor hydrogen acts as a shallow donor (H^+) increasing the number of free electrons in the conduction band [16]. The effect of hydrogen is determined by its high reactive properties. It can form oxygen vacancies (V_o), as well as bind to intrinsic defects of NCs and dopant ions, forming hydrogen complexes [17]. These complexes, as a rule, have unpaired electron spins and their own magnetic moment. Therefore, the EPR spectra of these samples will have additional contributions due to the presence of such hydrogen complexes, which increase the intensity of the background line.

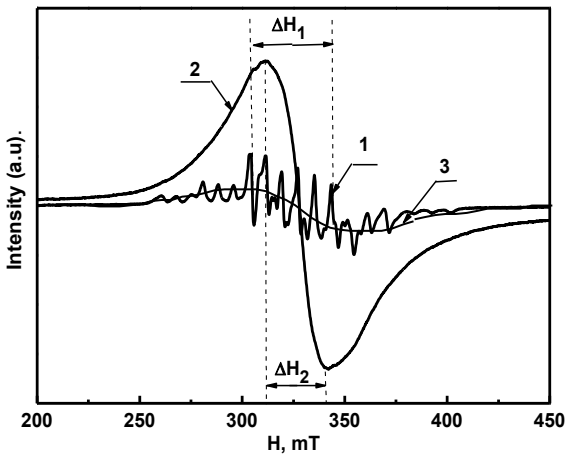

Fig. 7. EPR spectra of the ZnO:Mn (2%) NC sample: 1– after annealing at T = 850˚C (20 min.) in air, 2 – after further annealing in a mixture of hydrogen and nitrogen gases in the ratio $H_2/N_2 \sim 0.3$, 3 – a broad background absorption line caused by the exchange interaction of Mn^{2+} impurity ions in the spectrum 1.

III. Optical, structural and radiospectroscopic studies of ZnO/MnO nanostructures

Characteristics of the studied samples: K1 – undoped ZnO NCs, K2 – ZnO:Mn NCs (2 at. %), K3 – ZnO:Mn NCs (4 at. %). The samples were synthesized under the same technological regimes: synthesis temperature T=550°C; liquid flow rate – 20 l/h; concentration of the base component in the liquid (zinc nitrate) C=5%. Sample K4 – ZnO:Mn NCs (2 at. %) was synthesized in the same regime as sample K2, but with a change of one technological parameter – increase the liquid flow rate by two times – to 40 l/h.

Experimental methodology.

Raman spectra were excited with 457 nm solid-state laser and acquired using a single-stage spectrometer MDR-23 (LOMO) equipped with a cooled CCD detector (Andor iDus 401, U.K.). The laser power density on the samples was less than 10^3 W/cm^2 to preclude any thermal or photoinduced modification of the samples. A spectral resolution of 4 cm^{-1} was determined from the Si phonon peak width of a single crystal Si substrate. The Si phonon peak position of 520.5 cm^{-1} was used as a reference for determining the position of the peaks in the Raman spectra of ZnO and ZnO:Mn nanostructures.

Photoluminescence (PL) spectra were recorded using a spectral complex based on an MDR-3 diffraction monochromator (LOMO) (inverse linear dispersion 2.6 nm/mm) under laser excitation from a pulsed nitrogen laser with a wavelength of 337 nm at room temperature (300K) and liquid nitrogen temperature (77 K).

IV. Results and discussion

Raman spectra. Fig. 8 shows the Raman spectra of the undoped ZnO (K1) sample and ZnO samples doped with Mn of different content: K2 (2 at.%); K3 (4 at. %); K4 (2 at.%) (2 times higher liquid rate). It can be seen from the figure that Raman spectrum of the undoped ZnO sample (K1) contain bands with frequencies of 98, 332, 438, 582 cm^{-1} which correspond to E_2 (low), E_2 (h) - E_2 (l), E_2 (high), A_1(LO) phonon frequencies characteristic for high-quality ZnO nanostructures.

The Raman spectra of Mn-doped ZnO NCs (K2-K4) change significantly. The bands related to ZnO NCs become less intense, and the bands from Zn-Mn-O are dominated in the spectrum. The band with a frequency of 573 cm^{-1} may belong to δ-MnO_2, since for α-MnO_2 and β-MnO_2 the frequency positions of the bands are much higher [18]. The band with a frequency of 675 cm^{-1} most likely belongs to the $ZnMn_2O_4$ compound [19].

Photoluminescence spectra. Fig. 9 – 11 demonstrate the photoluminescence spectra of undoped (K1) and doped (K2, K3, K4) ZnO NCs.

The structure of the PL spectra of ZnO NCs in the region of the fundamental absorption edge and impurity states in the energy band gap is determined by the radiative transitions involving free and bound excitons, as well as the recombination of charge carriers trapped by impurity centres. Analysis of the changes in the energy position and

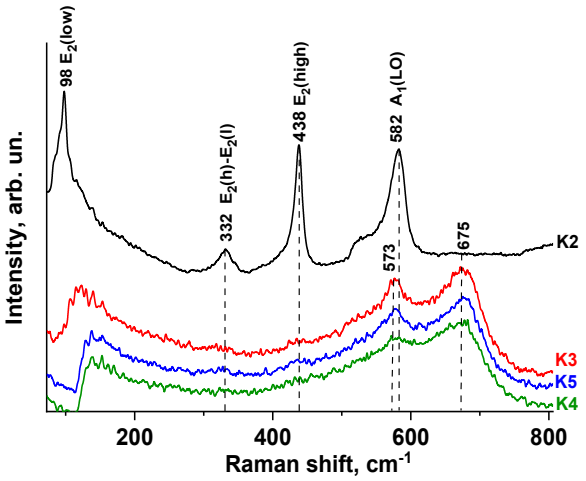

Fig. 8. Raman spectra of undoped ZnO (K1) sample and ZnO samples doped with Mn with different content: K2 (2 at.%); K3 (4 at.%); K4 (2 at.%) (2 times higher liquid rate).

intensity of the exciton bands of PL as a result of doping and other technological processes reveal the information about the perfection of the material crystal structure and the presence of defects that affect recombination processes. For example, in [20] as a result of comprehensive studies of the dependence of the optical band gap of ZnO NCs on the density of planar stacking defects using methods of wide-angle X-ray scattering and photoluminescence, it was found that the concentration of defects (1.6 x 10^{6}cm^{-1}) leads to a narrowing of the optical band gap from 3.37 eV to 3.27 eV. The expansion of the band gap to 3.52 eV is observed at a lower defect density (0.8 x 10^6 cm^1) with the quantum-size effects prevailing.

Fig. 9 presents the PL spectra measured at T = 300 K. It should be noted that the studied samples in the form of powders were packaged to prevent their contact with air. The most intense PL band is observed in the exciton region of the spectrum (λ_{max}= 380.6 nm) for sample K4. For other samples, emission bands in the exciton region was practically absent. As for the so called “impurity” region of the spectrum, for all samples the PL intensity at room temperature is rather weak. In our opinion, the obtained result - a significant increase of the intensity of the exciton PL for the sample K4 as a result of an increase in the flow rate of the liquid during the synthesis process - is interesting and requires additional research. Therefore, the presence of intense exciton PL is an evidence of a sufficiently high structural perfection of the material. This means that the optimal technological regimes for obtaining high-quality, structurally perfect ZnO NCs can be found, in particular, by changing the fluid flow rate during the synthesis process.

For a more detailed study of the nature of the PL bands in the exciton and impurity regions of the spectrum, PL spectra of ZnO NCs have been measured at liquid nitrogen temperature (T=77K).

Fig. 10 shows the PL spectra of the hermetically packed samples of ZnO NCs during the first cycle of measurements. It can be seen that exciton bands appear only for the undoped sample K1 and the sample K4 for which the liquid flow was increased to 40 l/h during the synthesis process. Such features indicate that these

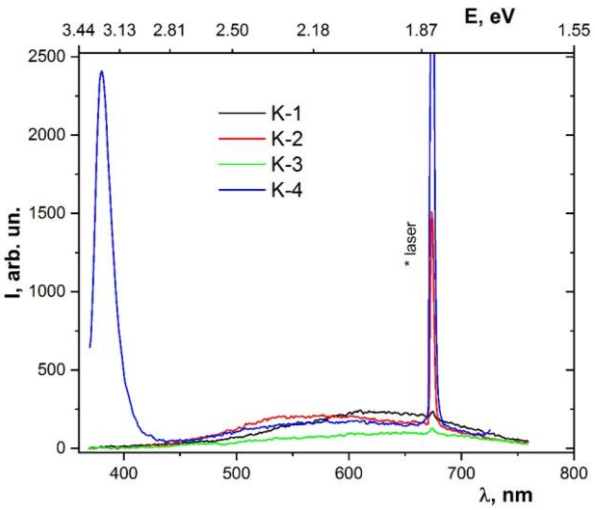

Fig. 9. PL spectra of ZnO NCs, $\lambda_{exc.}$ = 337 nm, T = 300K.

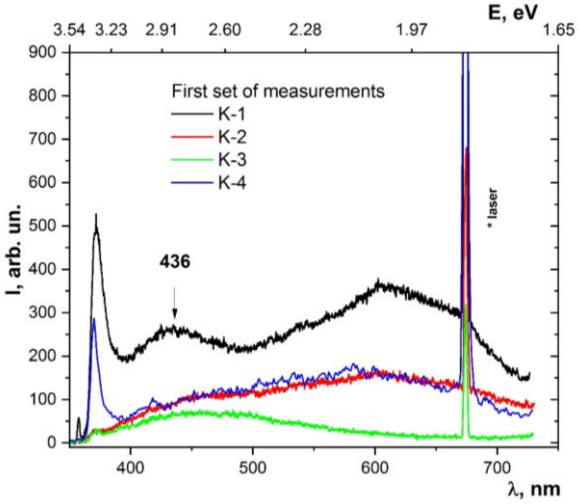

Fig. 10. PL spectra of ZnO NCs, which were recorded during the first cycle of measurements, $\lambda_{exc.}$ =337 nm, T = 77 K

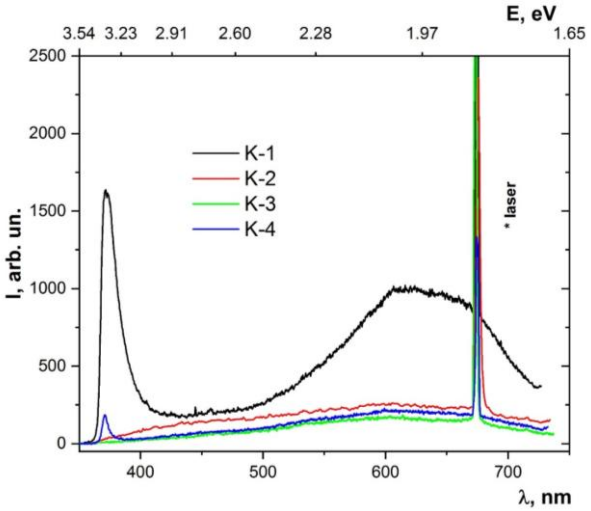

Fig. 11. PL spectra of ZnO NCs after staying in air for 10 min, $\lambda_{exc.}$ = 337 nm, T = 77 K.

samples are the most structurally perfect. Moreover, for sample K4 the exciton band is shifted to the short-wavelength region by approximately 1.6 nm compared to the undoped one, i.e. this sample is less defective than the undoped one. This result confirms the conclusion made above that the increasing of the liquid flow during the synthesis of ZnO:Mn NCs increases the structural perfection of nanocrystals.

Further, we consider the "impurity" PL. In this region, a band in the violet region of the spectrum with a maximum at λ = 436 nm (2.84 eV) is clearly defined. In [21] the detailed studies of the temperature dependence of the PL spectra of ZnO nanoneedle arrays grown on a silicon substrate by electrochemical deposition, as well as studies of EPR and X-ray photoelectron spectra, established that emission in the 436.0 nm region occurs with the participation of oxygen vacancies concentrated on the surface of the nanoneedle. The influence of intrinsic defects on the nature of PL bands in ZnO was determined in [22, 23]. It is emphasized in [23] that oxygen vacancies have a lower formation energy than interstitial zinc, which implies a higher concentration of oxygen vacancies.

For all samples, a broad structural PL band in the region of 500-700 nm (2.5 -1.7 eV) is observed on the long-wavelength side of the so called "violet" emission band. It consists of the so-called green, yellow, and red defect emission bands. The majority of researchers associated the green band with the presence of oxygen vacancies, in particular with transitions involving singly ionized (F^+) oxygen vacancies (V_O) [24]. The band in the region of 2.0 eV (yellow band) has been interpreted by a transition between a shallow donor and an acceptor with an energy level above the valence band [25]. The red PL band is often attribute to the presence of defects associated with interstitial zinc (Zn_i) [26] or a defect complex V_O-Zn_i [27].

It should be noted that the "violet" band is quenched approximately equally after the doping of ZnO NCs with Mn ions of 2% (samples K2 and K4) and 4% (sample K3), while the yellow band is quenched approximately twice for ZnO NCs doped with Mn ions of 2% and is almost completely quenched when ZnO NCs doped with Mn ions of 4% (Fig. 10). Therefore, an increase in the concentration of the Mn impurity leads to the blocking of radiative donor-acceptor transitions.

The samples under study were unpacked and exposed

to air for a short time to study the effect of oxygen adsorption on the PL spectra of ZnO powders. Fig. 11 shows the PL spectra of ZnO NCs after exposure to air for 10 min. It can be seen that the violet emission band with a maximum at λ = 436 nm disappears completely. This means that oxygen atoms fill the corresponding vacancies, which form the 436 nm PL band. It can be assumed that for ZnO NCs both undoped and doped with Mn ions, the PL band with a maximum of 436 nm is associated with oxygen vacancies on the surface of ZnO NCs (similarly to the results obtained in [21]).

It should be noted that we observe a decrease in the emission intensity upon Mn doping of ZnO NCs, which may be due to the enhancement of non-radiative recombination processes [28]. For example, similar intensity reduction effects were observed in ZnO nanorods doped with Mn and Co [29].

Conclusions

1. A technology for the synthesis of ZnO and ZnO:Mn nanocrystals by ultrasonic spray pyrolysis has been developed.

2. The defective near-surface layer in ZnO:Mn NCs has been reveal based on the analysis of the EPR spectra. Thermal annealing of samples at T = 850°C leads to the ordering of the crystal structure of ZnO:Mn NCs. It has been shown that the solubility limit of the Mn impurity is less than 2%.

3. Analysis of Raman spectra of synthesized samples demonstrate that ZnO:Mn NCs are covered with $ZnMn_2O_4$ and δ--MnO_2 shells.

4. A significant increase in the intensity of exciton photoluminescence for ZnO NCs caused by the improvement of the structural perfection of NCs is to be a result of increasing the liquid flow rate to 40 l/h during the synthesis process. Thus, the optimal technological regimes to form high-quality, structurally perfect ZnO NCs can be elaborated by changing the liquid flow rate during the synthesis process.

5. Most likely, the PL band with a maximum at 436 nm is associated with oxygen vacancies on the surface of ZnO NCs, as evidenced by the disappearance of this band after the samples were exposed to air for a short time (10 min) and, as a result, the adsorption of oxygen by ZnO NCs. The effect of moisture on the photoluminescence of ZnO NCs is also not excluded, but this issue requires additional study.

Kovalenko O.V. – Doctor of Physical and Mathematical Sciences, Professor, Head of the Department of Applied Radiophysics, Electronics and Nanomaterials;
Vorovsky V.Yu. – Head of the Laboratory of the Department of Applied Radiophysics, Electronics and Nanomaterials;
Berezovska N.I. – Candidate of Physical and Mathematical Sciences, Senior Researcher;
Dmytruk I.M. – Doctor of Physical and Mathematical Sciences, Professor of the Department of Experimental Physics;
Korbutyak D.V. – Doctor of Physical and Mathematical Sciences, Professor;
Yukhymchuk V. O. – Doctor of Physical and Mathematical Sciences, Professor, Head of the Department of Optics and Spectroscopy.

[1] D. Raoufi, *Synthesis and microstructural properties of ZnO nanoparticles prepared by precipitation method*, Renewable Energy, 50, 932 (2013); https://doi.org/10.1016/j.renene.2012.08.076.
[2] M. M. Ba-Abbad, A .A. H. Kadhum, A. B. Mohamad, M. S. Takriff, K. Sopian, *Optimization of process parameters using D-optimal design for synthesis of ZnO nanoparticles via sol-gel technique*, Journal of Industrial and Engineering Chemistry, 19(1), 99 (2013); https://doi.org/10.1016/j.jiec.2012.07.010.
[3] T. Wangensteen, T. Dhakal, M. Merlak, P. Mukherjee, M. H. Phan, S. Chandra, H. Srikanth, S. Witanachchi, *Growth of uniform ZnO nanoparticles by a microwave plasma process,* Journal of Alloys and Compounds, 509(24), 6859 (2011); https://doi.org/10.1016/j.jallcom.2011.03.161.
[4] B. W. Chieng, Y. Y. Loo, *Synthesis of ZnO nanoparticles by modified polyol method*, Materials Letters, 73, 78 (2012); https://doi.org/10.1016/j.matlet.2012.01.004.
[5] P. Rai, Y.-T. Yu, *Citrate-assisted hydrothermal synthesis of single crystalline ZnO nanoparticles for gas sensor application*, Sensors and Actuators B: Chemical, 173, 58 -65(2012); https://doi.org/10.1016/j.snb.2012.05.068.
[6] M. Vaghayenegar, A. Kermanpur, M. H. Abbasi. *Bulk syntheis of ZnO nanoparticles by the one-step electromagnetic levitational gas condensation method*. Ceramics International, 38(7), 5871 (2012); https://doi.org/10.1016/j.ceramint.2012.04.038.
[7] S. C. Tsai, Y. L. Song, C. S. Tsai, C. C. Yang, W. Y. Chiu, H. M. Lin, *Ultrasonic spray pyrolysis for nanoparticles synthesis*, Journal of Materials Science, 39, 3647 (2004). https://doi.org/10.1023/B:JMSC.0000030718.76690.11.
[8] O. V. Kovalenko, V. Yu. Vorovsky, *Dependence of magnetic properties of ZnO:Mn nanocrystals on synthesis conditions,* Journal of nano- and electronic physics, 14(3). 03030 (2022); https://doi.org/10.21272/jnep.14(3).03030.
[9] [9] O. V. Kovalenko, V. Yu. Vorovsky, O. V. Khmelenko, Ye. G. Plakhtii, *Peculiarities of doping of ZnO:Mn nanocrystals as during their synthesis by the aerosol pyrolysis method*, Journal of Physics and Electronics, 28(2), 91 (2020); https://doi.org/10.15421/332027.
[10] M. Hasan, Q. Liu, A. Kanwal, T. Tariq, G. Mustafa, S. Batool, M. Ghorbanpour, *A comparative study on green synthesis and characterization of Mn doped ZnO nanocomposite for antibacterial and photocatalytic applications*, Scientific Reports, 14, 7528 (2024); https://doi.org/10.1038/s41598-024-58393-0.

[11] D. Toloman, A. Mesaros, A. Popa, O. Raita, T. D. Silipas, B. S. Vasile, O. Pana, L. M. Giurgiu, *Evidence by EPR of ferromagnetic phase in Mn-doped ZnO nanoparticles annealed at different temperatures*. Journal of Alloys and Compounds, 551, 502 (2013); https://doi.org/10.1016/j.jallcom.2012.10.183.

[12] S. Bhattacharyya, D. Zitoun, A. Gedanken, *Electron Paramagnetic Resonance Spectroscopic Investigation of Manganese Doping in ZnL (L = O, S, Se, Te) Nanocrystals*, Nanoscience and Nanotechnology Letters, 3(4), 541 (2011). https://doi.org/10.1166/nnl.2011.1208.

[13] H. Zhou, D. M. Hofmann, A. Hofstaetter, B. K. Meyer, *Magnetic resonance investigation of Mn^{2+} in ZnO nanocrystals*. J. Appl. Phys., 94(3), 1965 (2003). http://dx.doi.org/10.1063/1.1586986.

[14] O. V. Kovalenko, V. Yu. Vorovsky, O. V. Khmelenko, *The effect of heat treatment on the magnetic properties of ZnO:Mn nananocrystals obtained by ultrasonic aerosol pyrolysis*. Functional Materials, 27(4), 687 (2020); https://doi.org/10.15407/fm27.04.687.

[15] O. V. Kovalenko, V. Yu. Vorovsky, O. V. Khmelenko, O. I. Kushnerov, *Effect of short-term heat treatment in the hydrogen on magnetic properties of ZnO:Mn nanocrystals*. Physics and Chemistry of Solid State, *23*(3), 569 (2022). https://doi.org/10.15330/pcss.23.3.569-574.

[16] E. V. Lavrov, F. Herklotz, J. Weber, *Identification of two hydrogen donors in ZnO,* Phys. Rev. B, 79, 165210 (2009); https://doi.org/10.1103/PhysRevB.79.165210.

[17] D.M. Hoffmann, A. Hofstaetter, F. Leiter et al., *Hydrogen: A Relevant Shallow Donor in Zinc Oxide*, Phys. Rev. Lett., 88 (4), 045504 (2002); https://doi.org/10.1103/PhysRevLett.88.045504.

[18] B. Yin, S. Zhang, H. Jiang, F. Qu, X. Wu, *Phase-controlled synthesis of polymorphic MnO_2 structures for electrochemical energy storage*, J. Mater. Chem. A, 3, 5722 (2015); https://doi.org/10.1039/C4TA06943A.

[19] B. Hadzic, N. Romcevic, M. Romcevic, I. Kuryliszyn-Kudelska, W. Dobrowolski, U. Narkiewicz, D. Sibera, *Raman study of surface optical phonons in hydrothermally obtained ZnO(Mn) nanoparticles,* Optical Materials, 58, 317, (2016); https://doi.org/10.1016/j.optmat.2016.03.033.

[20] F. Bertolotti, A. Tăbăcaru, V. Mușat, N. Ţigău, A. Cervellino, N. Masciocchi, A. Guagliardi, *Band Gap Narrowing in Silane-Grafted ZnO Nanocrystals. A Comprehensive Study by Wide-Angle X-ray Total Scattering Methods*, J. Phys. Chem. C, 125(8), 4806 (2021); https://doi.org/10.1021/acs.jpcc.0c10502.

[21] B. Cao, W. Cai, H. Zeng, *Temperature-dependent shifts of three emission bands for ZnO nanoneedle arraus*, Appl. Phys. Letters, 88, 161101 (2006); https://doi.org/10.1063/1.2195694.

[22] A. F. Kohan, G. Ceder, D. Morgan, Chris G. *Van de Walle, First-principles study of native point defects in ZnO*, Phys. Rev. B, 61, 15019 (2000); https://doi.org/10.1103/PhysRevB.61.15019.

[23] F. Oba, S. R. Nishitani, S. Isotani, H. Adachi, I. Tanaka, *Energetics of native defects in ZnO*, J. Appl. Phys., 90(2), 824 (2001); https://doi.org/10.1063/1.1380994.

[24] P. Zhan, W. Wang, C. Liu, Y. Hu, Zh. Li Zh, Zhang, P. Zhang, B. Wang, X. Cao, *Oxygen vacancy–induced ferromagnetism in un-doped ZnO thin films*, J. Appl. Phys. 111, 033501 (2012); http://dx.doi.org/10.1063/1.3679560.

[25] [25]. C. Gaspar, F. Costa, N. Monteiro. *Optical characterization of ZnO*. Journal of Materials Science: Materials in Electronics. 12, 269–271 (2001).

[26] F. Güell, P. R. Martínez-Alanis, *Tailoring the Green, Yellow and Red defect emission bands in ZnO nanowires via the growth parameters*. Journal of Luminescence, 210, 128 (2019); https://doi.org/10.1016/j.jlumin.2019.02.017.

[27] Y. N. Chen, S. J. Xu, C. C. Zheng, J. Q. Ning, F. C. C. Ling, W. Anwand, G. Brauer, W. Skorupa, *Nature of red luminescence bad in research-grade ZnO single crystals: A "self-activated" configurational transition*. Applied Physics Letters. 105, 041912 (2014); http://dx.doi.org/10.1063/1.4892356.

[28] R. Karmakar, S. K. Neogi, Aritra Banerjee, S. Bandyopadhyay, *Structural; morphological; optical and magnetic properties of Mn doped ferromagnetic ZnO thin film,* Applied Surface Science. 263, 671 (2012); https://doi.org/10.1016/j.apsusc.2012.09.133.

[29] B. Panigrahy, M. Aslam, D. Bahadur, *Aqueous Synthesis of Mn- and Co-Doped ZnO Nanorods,* J. Phys. Chem. C, 114(27), 11758 (2010); https://doi.org/10.1021/jp102163b.

О. В. Коваленко[1], В.Ю. Воровський[1], Н.І. Березовська[2,3], І.М. Дмитрук[2,3], Д.В. Корбутяк[4], В. О. Юхимчук[4]

Оптичні, структурні та радіоспектроскопічні дослідження наноструктур ZnO/MnO, синтезованих методом ультразвукового піролізу аерозолю

[1]Дніпровський національний університет імені Олеся Гончара, м.Дніпро, kovalenko.dnu@gmail.com; kriotech2@ukr.net
[2]Київський національний університет імені Тараса Шевченка
[3]Інститут фізики НАН України,nataliya.berezovska@knu.ua, igor_dmytruk@knu.ua;
[4]Інститут фізики напівпровідників імені В. Є. Лашкарьова НАН України, dmytro.korbutyak@gmail.com, v.yukhymchuk@gmail.com

Розроблено технологію синтезу нанокристалів (НК) ZnO та ZnO, легованого магнітною домішкою Mn у концентраціях 2% та 4%, методом ультразвукового піролізу аерозолю. Структурні, морфологічні та оптичні властивості синтезованих НК ZnO були досліджені методами рентгенівської дифракції, скануючої електронної мікроскопії, електронного парамагнітного резонансу (ЕПР), спектроскопії комбінаційного розсіювання та фотолюмінесценції. Дефектний приповерхневий шар у НК ZnO:Mn був ідентифікований на основі аналізу спектрів ЕПР. Термічний відпал зразків при T = 850°C призводить до впорядкування кристалічної структури НК ZnO:Mn. Межа розчинності домішки Mn становить менше 2%. Аналіз спектрів комбінаційного розсіювання показав, що НК ZnO:Mn покриті оболонками $ZnMn_2O_4$ та δ--MnO_2. Значне збільшення інтенсивності екситонної фотолюмінесценції для наночастинок ZnO, спричинене покращенням структурної досконалості наночастинок, є результатом збільшення швидкості потоку рідини до 40 л/год під час процесу синтезу. Таким чином, оптимальні технологічні режими для формування високоякісних, структурно досконалих наночастинок ZnO можна розробити, змінюючи швидкість потоку рідини під час процесу синтезу.

Ключові слова: Оксид цинку, нанокристали, магнітні домішки, дефекти, ультразвуковий розпилювальний піроліз, рентгенівська дифракція, електронний парамагнітний резонанс, комбінаційне розсіювання, фотолюмінесценція